Automatic Tools for Diagnosis Support of Total Hip Replacement Follow-up

Laura FLOREA, Corneliu FLOREA, Constantin VERTAN, Alina SULTANA
Image Processing and Analysis Laboratory, Politehnica University of Bucharest, Romania
laura.florea@upb.ro

***Abstract*—Total hip replacement is a common procedure in today orthopedics, with high rate of long-term success. Failure prevention is based on a regular follow-up aimed at checking the prosthesis fit and state by means of visual inspection of radiographic images. It is our purpose to provide automatic means for aiding medical personnel in this task. Therefore we have constructed tools for automatic identification of the component parts of the radiograph, followed by analysis of interactions between the bone and the prosthesis. The results form a set of parameters with obvious interest in medical diagnosis.**

***Index Terms*—biomedical image processing, feature extraction, image enhancement, prosthetics, X-rays.**

I. INTRODUCTION

The idea of total hip prosthesis was born before the 1950s and evolved towards the total hip prosthesis universally used today, composed of a stem and an acetabular component. The replacement procedure known as total hip arthroplasty (THA) became a well-known and highly developed technique to reduce pain in arthrotic and arthritic hips.

Taking into account the data existing in the Nationwide Inpatient Sample (NIS) [1] the hip replacement procedures increased by about 32% (from 290,700 procedures to 383,500 procedures per year), between 1997 and 2005 in US alone. Kurtz et al. [2] used this data to make projections and to analyze the population-based outcomes of THAs, estimating that by 2030 the demand for primary THAs will grow by 174% to 572,000 procedures per year.

In the majority of cases, after a hip replacement procedure, the patient is able to fully recover, although at certain times complications may appear. The hip prostheses procedures require a continuous, regular and careful follow-up and monitoring, in order to detect failures. Wear is an important factor in failure, as is aseptic loosening, which is an indication for revision surgery in up to 20% of the primary THA's. Aseptic loosening of a THA is the result of a combination of bio-mechanical and chemical factors: the weakening of the bone resulting from bone resumption because of particle disease; the material strain in the interface of prosthesis and bone; the failure of the ingrowths in improperly fitted un-cemented prostheses; the inadequate stress transfer of prosthesis to bone [3].

A key issue in the prosthesis check-up is the need of consulting very specialized medical personnel, which is concentrated in a few centers, unlike the geographical spread of X-ray machines and general practitioners. Under these circumstances, the implementation of computer-assisted tools for supporting the diagnosis is of great interest, since it may help distribute some of the regular, normally evolving cases away from the THA-performing medical centers and orthopedic surgeons.

In this paper we present the results of our efforts to produce computer based automatic tools for the support of the diagnosis in prosthesed hip area. Consequently, the remainder of the paper is organized as follows: the next section deals with the problem of turning analogue film radiographs into digital images; section III describes the prosthesis and bone segmentation procedures which are further used, as we will describe in section IV to produce clinical relevant measurements.

II. DIGITIZATION AND VISUALIZATION

Although modern technology provides means and apparatus for digital X-ray acquisition, due to cost and time evolution considerations, such an option is not always possible. In less economically developed areas, bone system visual investigations still rely on analogue X-ray images. Moreover, the analogue radiographies acquired in the past represent valuable information for current medical investigations. As detailed in section IV A, the majority of our data came in analogue form; hence, we aimed a low cost alternative digital acquisition scheme, which implies photographing the radiographic film with a regular, consumer grade, digital still camera. Such an approach has a major drawback: the low dynamic range of a digital still camera output reduces the quantity of information available in a radiograph. This means a loss of details existing in the original image and obviously the problem has to be dealt with.

In order to study the behavior of the femoral components of the hip prosthesis, the needed image can be limited to the immediate area surrounding the prosthesis stem, corresponding to an area of some 300cm^2 of radiographic film. From the medical practice it comes that we should reliably measure and represent details as small as 0.1 mm within the area of interest. That leads to the constraint of using a minimal 10pixels/mm (250ppi) resolution, implying the use of a digital still camera with at least 4Mpixels sensor. This is easily achievable by a reasonable consumer digital still camera.

Yet, the digital camera cannot provide the equivalent dynamic range of the X-ray film. The spatial resolution of an analogue X-ray image is given by the grain density of the film, which is typically at some 10^8grains/cm^2, yielding a

The work has been co-funded by the Sectoral Operational Programme Human Resources Development 2007-2013 of the Romanian Ministry of Labour, Family and Social Protection through the Financial Agreement POSDRU/89/1.5/S/62557 and POSDRU/89/1.5/S/64109.

This work has been co-funded by the CEEX VIASAN grant 69/2006.

Digital Object Identifier 10.4316/AECE.2011.04009

dynamic range of approximately 36dB [4]. The images acquired by a digital still camera have a resolution given by the camera sensor size (upper limited at some 10^7pixels) and the size of the imaged area. Such images exhibit a typical dynamic range of some 24dB to 32dB (depending on the image mode - color or RAW).

Two approaches were considered to fix the loss of information in digitized images of the hip area. One is to combine frames acquired with different exposures and to process the results [5]. Another solution uses only one initial image and a pixel ordering technique [6]. The resulting quantization over-samples the output space, such that the details visibility is increased. The two methods will be shortly described from a comparative point of view.

A. X-ray image dynamic range increase by combining multiple scene instances

The straightforward solution to the problems generated by the reduced dynamic range of the digital still camera is to combine multiple images of the same scene, taken under various settings (usually different shutter speeds). This approach is known as bracketing. The underlying idea is that each of the images that are to be combined captures with high quality only a certain part of the scene color (or grayscale) gamut (as imposed by the settings of the camera). The algorithm selects, for each pixel of the spatial support of the scene, the acquired image that provides the best value. That selection is based on the assumption that all the images are perfectly aligned.

Traditionally, there is a first step of image registration that ensures the perfect alignment of the individual frames. However this has high computational cost and there is no method with 100% accuracy. Thus a mechanical device that impedes the miss-alignments (like placing the camera on a tripod) is preferred.

The second step is the actual dynamic range increasing. The approach becomes more and more common and is widely described in literature [7].

The input data is a set of three photographs, namely I_1, I_2, I_3 acquired with different exposures, $Ev_1 = 0$, $Ev_2 = -1$, $Ev_3 = +1$. Ev is a logarithmic measure for relative exposure; $Ev = 0$ is given to a photograph, when the exposure time and aperture balance the illumination of the scene and internal camera amplification in order to have a near uniform resulting histogram [8]. An image with $Ev = -1$ is acquired with half of the normal exposure time and, therefore, is under-exposed. $Ev = +1$ is obtained for an image with double of exposure time and, thus, is over-exposed. Each such image correctly records one part of the scene's gamut and is less accurate elsewhere: the under-exposed image records correctly the upper part of the gamut, while the lower part is degraded by quantization error and noise; the normal-exposed image is accurate in the center part of the gamut and the over-exposed image is accurate in the lower part, while the upper range is degraded by saturation. This information may be encoded by a set of weights, ω. A formal derivation of these weights may be found in [5], while an example is presented in figure 1.

The fusion method of the three images is direct. The saturated pixels and the noise-corrupted pixels are discarded, and we simply average using the discussed weights, the values of the remaining pixels across the set of acquired images. The pictures with normal exposure are the reference for the image content. The pixels arriving from under or over-exposed images add details. The operation is performed independently for each pixel in the resulting image.

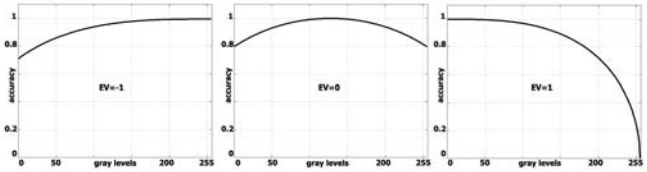

Figure 1. The weights, ω, that encode the information accuracy (on the Y axis, in the [0,1] range) in an under-exposed image (*Ev=-1*, left hand plot), normal-exposed image (*Ev*=0, center plot) and over-exposed image (*Ev*=+1, right hand plot), with respect to image intensities (on X axis, given in [0,255] range). The weights correspond to a consumer digital still camera.

The mixing of the input frames (I_1, I_2, I_3) at (l,m) location takes the form of a convex combination:

$$I_{HDR}(l,m) = \frac{1}{C(l,m)} \otimes \left[I_\omega^1 \oplus I_\omega^2 \oplus I_\omega^3 \right] \tag{1}$$

where :

$$I_\omega^k = \omega\left(Ev(k), I_k(l,m)\right) \otimes I_k(l,m)$$
$$C(l,m) = \sum_{k=1}^{3} \omega\left(Ev(k), I_k(l,m)\right) \tag{2}$$

In the above equations, the set of weights, ω, are predefined and are plotted in figure 1.

It has been shown, [5], that for this specific problem, if the scalar multiplication, $\otimes$, and the addition, $\oplus$, are implemented according to a non-linear image processing model, like the one proposed by Jourlin and Pinoli [9], the level of details in the resulting image is higher. A set of the initial three frames and the resulting high dynamic range (HDR) image is to be found in figure 2.

B. X-ray image dynamic range increase by total pixel ordering

The bracketing method described in the subsection above has the disadvantage of requiring several frames hence increasing the algorithm memory requirements. The natural way to avoid such a problem is the use of a single image, reasonably well exposed, and to review the dynamic range increase problem within an image enhancement framework.

Basically, we can view the dynamic range increase as the creation of significantly more different pixel values that the number of different pixel values available in the initial image. This cannot be performed by simple, point image enhancement operations, such as the classical histogram equalization or histogram stretching [1], but requires the segregation of same-valued pixels according to their local statistics. In some way, we replace the multiple luminance values available at each pixel location from multiple acquisitions of the scene (as used in the bracketing approach) by data computed in some spatial neighborhoods, yielding to the association of a feature vector to each image pixel. The pixels are then ordered according to their feature

vectors and, based on the resulting string the pixels are assigned new, increasing gray level values. This is the approach introduced in [11] for histogram specification.

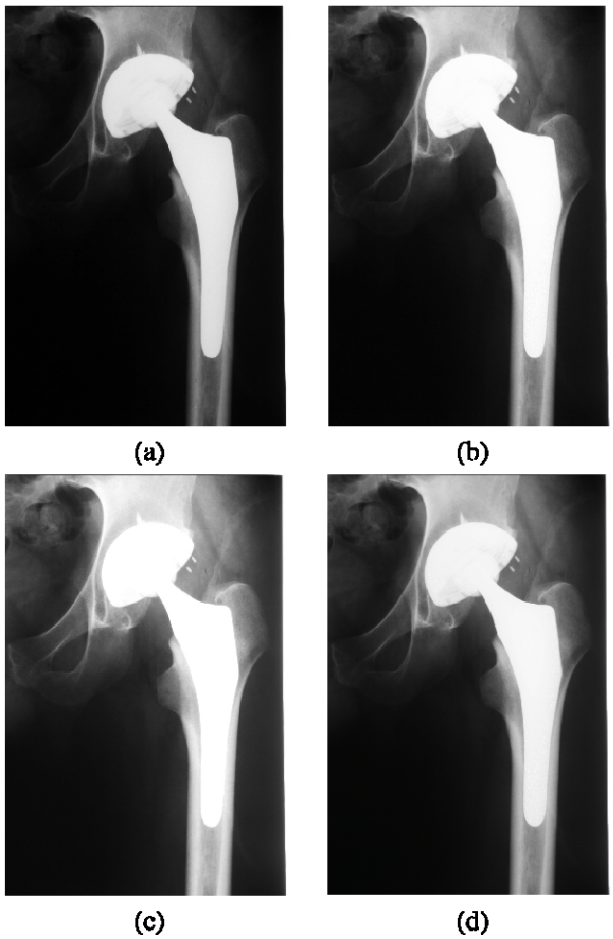

Figure 2. Digital still camera acquisition of radiographic film image of total hip prostheses: (a) under-exposed, (b) normal-exposed and (c) over-exposed image. All images are 8 bits per pixel (bpp) luminance images of the original 12 bpp equivalent film. The resulting HDR image (d) is plotted simulating 12bpp by using highly unsaturated colors (as explained in subsection II. C).

Initially, the specified histogram is either flat (yielding to a perfect histogram equalization) or a stretched variant of the original histogram of the image, but with the same number of bins, corresponding to the same number of different gray levels in the resulting image. In order to increase the dynamic range of the resulting image, we will use a different approach by specifying a histogram with more bins (and thus more different gray levels in the resulting image) than the number of bins in the original image. This target histogram will be obtained by interpolating the histogram of the original image.

Let *I* be the initial image. Each pixel (*l*,*m*) from the image *I* is mapped to a feature vector $\vec{g}(l,m)$, composed by:

$$\vec{g}(l,m)=\left[g_1(l,m),g_2(l,m),g_3(l,m),...\right] \tag{3}$$

where $g_1(l,m)$ is the initial pixel value (in order to maintain the relative intensity ranking of pixels) and $g_k(l,m)$ with $k>1$ are the features computed in some neighborhoods of the current pixel. Let $\prec$ be the lexicographic ordering relation applied to the feature vectors $\vec{g}(l,m)$; two feature vectors verify the ordering relation $\vec{g}(l_1,m_1)\prec\vec{g}(l_2,m_2)$ if and only if:

$$\exists k,\begin{cases} g_i(l_1,m_1)=g_i(l_2,m_2) \\ g_k(l_1,m_1)<g_k(l_2,m_2)\end{cases},1\le i<k \tag{4}$$

The choice of specific features $g_k(l,m)$ is imposed by the desired appearance of the final image. The use of local averages, as suggested in [11], as a reference choice, will favor the pixels located in uniform areas and will slightly blur the edges. In order to enhance the overall edge visibility, we shall use some different form for the $g_k(l,m)$ features, as suggested by the following observations.

Considering the case of two pixels that have the same value, their difference is imposed by the relative order of their features. If the pixels are located in a uniform region, then their supplementary features should be zero. If the pixels are located within a non-uniform area, then the contrast of that area should be increased. It is well known that the human eye is sensitive to luminance contrast and two regions of the same shape and gray level will be seen differently based on the gray level of the background: if one of the shapes is placed on a lighter background (higher gray level), it will appear darker than the other one. Thus, in the non-uniform areas, the pixel that has a lower gray level than the local mean will be made even darker; the pixel that has a greater gray level compared to the local mean will be made lighter.

We define the features $g_k(l,m)$ in $(2k+1)\times(2k+1)$ neighborhood as follows:

$$g_k(l,m)=\alpha(\sigma)sign\left(I(l,m)-\overline{I_k(l,m)}\right) \tag{5}$$

where $\overline{I_k(l,m)}$ is the local mean (within the $(2k+1)\times(2k+1)$ neighborhood) and α is a function of the local standard deviation σ. An intuitive choice for α may be:

$$\alpha(\sigma_k)=\frac{\sigma_k}{\sigma_{\max}} \tag{6}$$

where $\sigma_{\max}$ is the maximal standard deviation within the image (computed at each pixel location within the $(2k+1)\times(2k+1)$ neighborhood).

One can decide the neighborhood is uniform if the variance is very small, even if it is not zero. In this case the α factor can be:

$$\alpha(\sigma_k)=\begin{cases} 0, & \sigma_k(l,m)\in[0,\sigma^*); \\ \dfrac{\sigma_k(l,m)-\sigma^*}{\sigma_{\max}-\sigma^*}, & \sigma_k(l,m)\in[\sigma^*,\sigma_{\max}); \end{cases} \tag{7}$$

where σ^* is the maximum value of the variance for which the neighborhood is considered uniform.

The described method was applied using a three-dimensional feature vector on the X-ray image captured under an automatic exposure, as the one presented in figure 3 (a). The result of the method is shown in figure 3 (b). In figure 3(c) the differences between the original image

multiplied by 2^2 and the HDR image obtained by pixel ordering method can be seen. As desired, the bigger the local contrast is, the bigger the differences.

a) b) c)

Figure 3. (a) Original image. (b) Image resulting after total ordering method with $\sigma^* = (\sigma_{\max} - \sigma_{\min})/15$. The resulting HDR image is plotted with 10bpp. c) The difference between the original image multiplied with 2^2 and the resulted HDR image.

C. Visualization and Evaluation

Both methods have been configured to produce HDR images with 12bpp. The 12bpp gray level images were displayed on usual RGB color displays using an extension of the classical gray level map via highly unsaturated colors that match the needed luminance levels that uniformly sample the luminance range. Indeed, the human visual system is unable to distinguish colors for which the difference within the maximal and minimal RGB components is small (less than 5 units on the 256 units scale). As such, the 4096 gray levels needed for the 12bpp representation are obtained from the 256 classical (and exact) gray levels and 3840 highly unsaturated colors.

For the evaluation of HDR images, even that several objective methods like the value of actual dynamic range or entropy are at hand, we considered that none of them is consistent with orthopedist or radiologist experimented opinion, which under these circumstances has to be taken as ground truth. Expert's opinion concluded that both methods produce more information that the original, normal-exposed images and the method involving multiple frames is better. Also it was in their opinion that even differences between original analog radiograph and the digital counterparts do exist, they do not alter the main features of the image and the consequent diagnosis will have the same accuracy as inspecting the original analog radiographs.

III. Prosthesis-Bone Segmentation

As mentioned in the introduction, we aimed at supporting the follow-up diagnosis. In such a case, the key feature is the accurate estimation of the prosthesis stem fit within the femoral bone [12]. But this may only come after the identification of the three major parts in the hip area: the soft tissue, the bone and the prostheses. This separation is in fact an image segmentation problem.

The goal of the image segmentation is the extraction of distinct objects (regions) from the original image [10]. The objects are defined according to the specific field of application and are usually described by some uniformity criterion. In this particular application we are primarily interested in the segmentation of the hip prosthesis, and, more precisely, in the segmentation of its stem (femoral component).

The envisaged problem is known and we can identify precursors of the proposed solutions. Segmentations of radiographic images of bone from the hip area, but without prostheses have been proposed by Dong, [13], or by Ying, [14], using contour detectors. Closer to the subject of this paper we consider the solutions proposed by Hatfield et al., [15], Kerrigan et al. [16], [17], which shapes the waist hip cartilage by ellipses; unfortunately the type of prosthesis used is cemented, leading to perfect fixation inside the femoral bone, hence a different pathology; also we aimed at computational more simple solutions.

To resolve the issue of radiographic image segmentation, we have addressed several methods such as:

- Histogram based segmentation both by empirical or adaptive thresholding (Otsu [18], Kitler [19]);
- Segmentation in the characteristics space by Fuzzy C-Means algorithm [20];
- Segmentation by Mean-Shift algorithm [21];
- Segmentation algorithm using Expectation-Maximization (EM) [22];
- Contour oriented segmentation using gradient, compass, Sobel [23], Harris [24] or Canny [25].

All these methods have been evaluated. The best results for identifying the prosthesis were found with EM algorithm and Canny contour operator. However, these general algorithms and their direct use provide a rough segmentation of the images. We are interested in the separation of the bone and, even more, the separation of the medullar channel. In order to do that and to achieve better results, another segmentation algorithm was developed. This algorithm starts at the results achieved by EM or Canny and adapts them to the problem specificity. All these algorithms will be discussed in the next subsections.

A. Region Oriented Segmentation

A histogram of a typical prosthesed hip area radiographic image is shown in figure 4. It can be seen that the upper histogram mode corresponds to the prosthesis (the foreground) and to some parts of the bone (from both the acetabulum and the femur), while the middle histogram mode relates to the bone mass. Thus, if the separation thresholds can be reliable and automatically detected, then three-class thresholding methods [26] could be effective for the segmentation of the prosthesis stem.

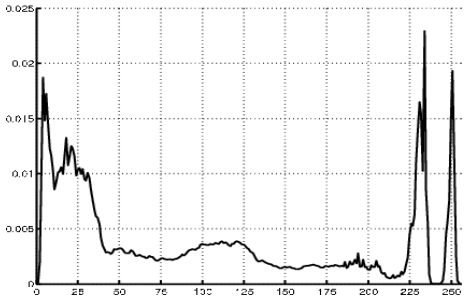

Figure 4. Histogram of the image from figure 5 (a).

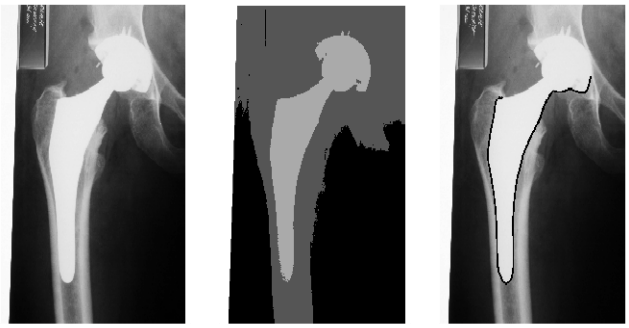

(a) (b) (c)

Figure 5. (a) Original image; (b) EM segmented image; (c) Prosthesis stem edge extracted by Canny algorithm from the original image.

Automatically finding the optimal thresholding value that correctly extracts the foreground is a problem widely studied in literature [27]. One of the histogram based segmentation techniques that leads to good results in our case implies the use of the Expectation-Maximization (EM) algorithm. The EM algorithm [28] is a classical method used in statistics to find the maximum likelihood estimates of a set of parameters that best fits the available data. In our case we assumed that the image data is generated by a mixture of three classes (prosthesis, bone, soft tissue), with each class being characterized by a Gaussian probability density function with mean μ_i and standard deviation σ_i, $N(\mu_i, \sigma_i)$ (with $i = 1,2,3$). Each class has its own weight ω_i, determined by the number of pixels in that class denominated by the total number of pixels, and the image probability density function is modeled by a mixture of Gaussians:

$$H = \sum_{i=1}^{3} w_i N(\mu_i; \sigma_i) \tag{8}$$

The EM algorithm will iterate until it finds the set of parameters that best fits the image histogram. Once the parameters are set, the class membership of each pixel is found by a simple maximum likelihood rule. An EM-segmented hip radiography is presented in figure 5 (b).

B. Contour Oriented Segmentation

Edge oriented image segmentation takes into account the spatial distribution of the pixels [29], looking for pixels related to spatial gray level discontinuities. Edge detection is based on local contrast, which seems more suitable for separation of the prostheses from the bone. Several techniques are at hand. Basic gradient operators, second-order derivative operators, phase congruency methods can be used for edge detection. But Canny operator [25] proved to be the most common and effective choice. We shall focus on it, since it provides the best results in our case.

A common choice [29] for the implementation of the Canny operator consists of the following steps:

- Gaussian smoothing to reduce the noise (which may be implemented by convolution with a Gaussian kernel);
- Sobel operator for edge detection;
- Non-maxima suppression used for locating the highest magnitude points in an edge map while suppressing the other;
- Threshold with hysteresis to connect edge points and therefore to provide continuous contours.

The Canny operator has been found very reliable in separating the prostheses stem from the bone. An example of Canny edge detection within a hip X-ray is presented in figure 5 (c). As one can easily notice, the edges of the stem are well detected.

C. Robust segmentation of the prosthesed hip images

A more efficient segmentation of the images should consider supplementary information about the content of the image to be segmented. For example we know that the prosthesed hip images will contain a central area with very light gray levels that corresponds to the prosthesis. The approximate shape of the prosthesis is also known. Around the prosthesis there might be a darker area - the medullar channel. On the borders of the image, soft tissue region will form a very dark, sometimes black area. All such information, although sometimes vague, may be placed in the segmentation algorithm. In the following we will describe an algorithm for segmenting radiographic images with prosthetic hip starting from the segmentation results already obtained by EM or Canny segmentation and taking into account the particularities of our images.

This segmentation method is based on image analysis of linear sections perpendicular to the femur (i.e. analyzing rows from the image if the femur is vertical). It requires a rough segmentation of this zone and analysis of its orientation. The rough segmentation step can be one of the algorithms discussed in the previous subsections: EM or Canny.

Using the rough segmentations results, the orientation of the prosthesis contour and its division into Gruen zones (see figure 6) can be inferred easily using geometrical considerations.

Further, the algorithm for segmenting the femoral area will investigate each linear section perpendicular to the prosthetic stem in order to determine the limits (contours) of the bone and of the medullar channel (where they exist). It will first define a maximum distance of search. A typical linear section, which includes bone, medullar channel and the prosthesis, can be seen in figure 7. One can easily observe that the center belongs to the prosthesis (characterized by very high intensities). On both sides of this area there is a valley, which belongs to the gray levels of the medullar channel (a darker area in the radiographic image) that separates the bone from the prosthesis. At the extreme edges the graph has very small values, which is the soft tissue that is of no interest in the present application. In the case presented in figure 7, on the left side of the image one can see an area with very high luminance. This area belongs to a region where the negatoscope was not covered by the radiograph. This region should be ignored in future analysis of the image.

In the following we denote by x_j, with $j = 1,...,M$ the gray level values present in the linear section (perpendicular to the prosthesis stem). The proposed method consists of three main steps:

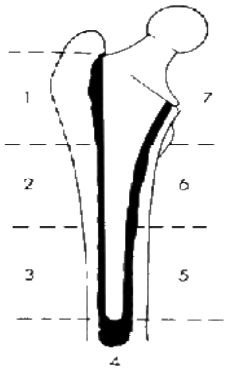

Figure 6. The 7 Gruen zones marked on a prostheses diagram.

1. Accurately determining the prosthesis limits, thus eliminating the possible small errors of the rough segmentation step done with EM or Canny algorithms. This step also allows us to make the rough segmentation on an image with lower resolution in order to increase the running speed of the algorithm;
2. Determining the outer limits of the bone;
3. Testing the existence of medullar channel followed by determination of its contours.

The bone and the prosthesis limits will be defined according to the gradient of the gray level profile of the linear section of the considered image. Thus the boundary between the prosthesis and the bone (or the medullar channel, if it exists) is characterized by the sharpest slope in the considered section. So, we define the left limit, p^{left} (the right one goes symmetrically) of the prosthesis stem as the abscissa point of the maximum variation of gray levels:

$$p^{left} = \arg\max_j \left(\frac{dx}{dj} \right) = \arg\max_j \left(x_{j+1} - x_j \right) \tag{9}$$

(9)

To eliminate errors that might occur due to the presence of different artifacts such as uncovered negatoscope area, markings on the X-ray analogue film, scratches etc., we used as starting points the roughly segmented prosthesis and we searched near these points. The search distance must be defined relative to the image resolution and to the size of the roughly segmented prosthesis. Of course, the final outcome will also depend on how fair the result of rough segmentation is.

The next step is to determine the outline points of the bone using a search area around the region of the prosthesis. The outline point of the femur on the left side of the prosthesis b^{left} is the one where the levels of gray start to show an increase:

$$b^{left} = \min\left(\arg_j \left(\left(x_{j+1} - x_j \right) > 0 \right) \right) \tag{10}$$

Next, we look inside the bone, to the medullar channel (if it exists) so to determine its contours. We will first define a set of conditions to be fulfilled to prove the existence of the channel. Thus, on each part of the prosthesis stem, the existence of the medullar channel is equivalent to the existence of a minimum boundary zone between the prosthesis contour and the outer limit of the bone. This zone, denoted by x^{left} and x^{right} can be mathematically defined as:

$$\begin{aligned} &x^{left} = x_j;\ j \in b^{left} \ldots p^{left} \Leftrightarrow \\ &\exists x_k \in x^{left}, \left(x_k - x_{k-1} \right) > T; \\ &x^{right} = x_j;\ j \in p^{right} \ldots b^{right} \Leftrightarrow \\ &\exists x_l \in x^{right}, \left(x_l - x_{l-1} \right) > T; \end{aligned} \tag{11}$$

where T is a predefined threshold.

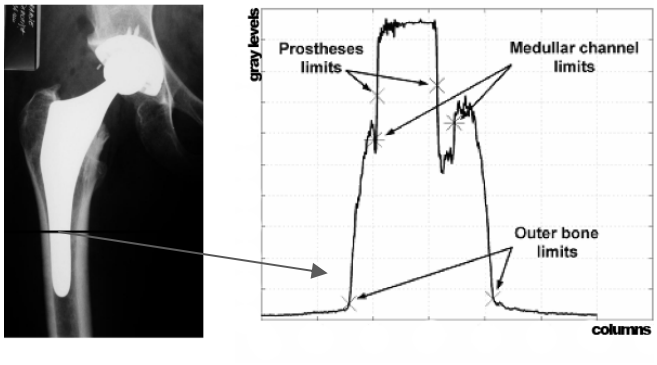

a) b)

Figure 7. a) Digital image of the prosthesis area. Marked with black is the line perpendicular to the prosthesis stem detailed in b). The points needed for segmentation are marked are shown.

If there is at least one point x_k then the point corresponds to the medullar channel in the left of the prosthesis. Similarly, if there is a point x_l there is medullar channel on the right side of the prosthesis.

The next step is to determine the medullar channel boundaries. For this step, several solutions are at hand. The best solution is to take the medullar channel limit as the point between the outer bone limit and the prosthesis limit where the gradient of gray levels exhibits a maximal decrease, respectively increase (in the right side of the prostheses):

$$\begin{aligned} c^{left} &= p^{left} - \arg\min_j \left(x_{j-1} - x_j \right); x_j \in x^{left} \\ c^{right} &= \arg\max_j \left(x_{j-1} - x_j \right) - p^{right}; x_j \in x^{right} \end{aligned} \tag{12}$$

Where the medullar channel is not found, its width will be set to zero.

Considering that linear sections perpendicular to the prosthesis were analyzed separately, one can apply a correction step that takes into account that in reality two successive contour points (prosthesis edges, or the inner and the outer bone) are not independent. As such, the errors can be reduced by a last filtering step, which was chosen as being a median one and imposed contour continuity.

At this point we provide a segmentation of the femoral area in four regions: soft tissue, bone with medullar channel and prosthesis. To construct an objective measure of correct segmentation method, a set of images were manually marked. Then we made measurements in respect to the manual marking, considered as ground truth. In table I we present the detection rate and false positives for all the segmented areas using as starting points the two methods of rough segmentation, EM and Canny respectively.

TABLE I. OBJECTIVE MEASUREMENTS - DETECTION RATE (D.R.) AND FALSE POSITIVES (F.P.) FOR THE SEGMENTATION OF PROSTHESIS, FEMORAL BONE AND MEDULLAR CHANNEL STARTING FROM THE TWO ROUGH SEGMENTATION METHODS DISCUSSED (CANNY AND EM).

Rough segmentation method	Measure	Robust with EM	Robust with Canny
Prostheses stem	D.R	71.8 %	99.1 %
	F.P	2.6 %	0.4 %
Femoral bone	D.R	68.6 %	96.9 %
	F.P	4.3 %	4.2 %
Medullar channel	D.R	65.1 %	94.5 %
	F.P	21.9 %	28.2%

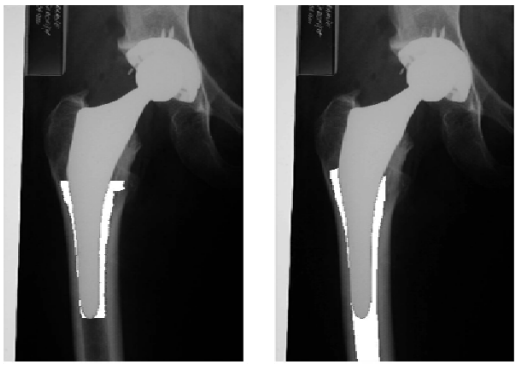

(a) (b)

Figure 8. (a) Segmentation of the medullar channel by the robust method described, (b) medullar channel manually marked.

In figure 8 one can see the results of the segmentation method described in this chapter on a radiographic image. The Canny operator was chosen to illustrate the rough segmentation step because it gives better results.

IV. CLINICAL RELEVANT MEASURES

When constructing a radiographic image analysis system to help medical staff, one must ensure that the statistical or topological measures are related to the clinical diagnosis. In the current section we present our proposals for the mentioned purpose. The actual computed measures focus on recording subtle information about the fixation of the prostheses stem inside the femoral bone.

As previously said, a problem that occurs in THAs is the inadequate fixation of the prosthesis. A serious consequence may be the bone breaking under the pressure of the femoral stem. We construct measures that can be used to estimate an overall score for the prosthesis stem fit inside the femoral bone. The investigated measures consist of the prosthesis - bone distance profile, the angle made by the prosthesis stem with the bone and the percentage of regions where the femur touches the prosthesis.

A. Database

In our study we have used 108 analogue radiographs from a total of 30 patients. There were between 2 and 5 different radiographs (acquired at different moments of time) for each patient. There were all antero-posterior images of the prosthesed hip area. From the different existing technological solutions for prostheses, our study focuses on the case of un-cemented prostheses with hydroxyl-apatite coating of the femoral stem. We have built digital images by photographing the film X-rays placed on a negatoscope.

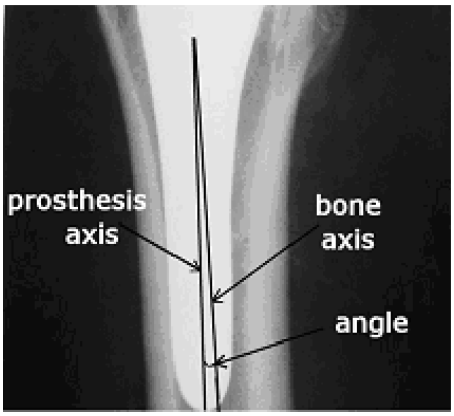

Figure 9. Radiographic hip prosthesis image with marked angle between the bone and the prostheses stem axis.

B. Bone- prosthesis angle

A parameter that can help determine a general measure of fit of the prosthesis in the medullar channel of the femur is the relative angle between the axis of the prosthesis stem and axis of the femoral bone. The axis of the bone is defined as the regression line of the pixels determined to be in the middle of the distance between the outer bone limits, while the axis of the prostheses is determined in respect to the prostheses edges.

A high value of this angle signals imminent danger, because the lower part of the prostheses stem apply high pressure on the bone, which can split or crack. The angle between the prosthesis and bone can be calculated for any segmentation method that separate bone pixels from those of prostheses. An example of representation of this angle is to be seen in figure 9.

TABLE II. RESULTS FOR ESTIMATING THE BONE - PROSTHESIS ANGLE WITH RESPECT TO THE MANUALLY MARKED IMAGES.

Segmentation method	Mean Square error[%]	Mean error [^{o}]
Robust with EM	6.9%	0.98^o
Robust with Canny	0.03%	0.13^o

A set of comparative results for the bone - prosthesis angle, depending on the rough segmentation method used, is presented in table II. The error is computed in respect to the manually marked images.

C. Region of adjacency

Another parameter of interest consists of the zones where the prosthesis is adjacent to the femur. A high percentage of such points correspond to the best match of the prosthesis in the femoral channel, while a low percentage is assigned to a weak attachment and may indicate impending fractures or osteolysis. A set of comparative results for the zone of adjacency, depending on the rough segmentation method used, is presented in table III. The error is computed in respect to the manually marked images.

TABLE III. RESULTS FOR ESTIMATING THE AREAS OF ADJACENCY WITH RESPECT TO THE MANUALLY MARKED IMAGES

Segmentation method	Mean Square error[%]	Mean error [pixels]
Robust with EM	0.35%	120 pixels
Robust with Canny	0.31%	108 pixels

D. Bone-prostheses distance profile

Another investigated aspect is the bone - prosthesis distance profile [6]. This profile can also be used to assess the fit of the prosthetic stem inside the medullar channel. If the prosthesis is not properly fitted inside the medullar channel, then its movement can bring discomfort and can cause damage or even breaking the bone.

A known clinical problem of hip prostheses is osteolysis. By rubbing the prostheses stem on the bone, its surface could loosen particles, which interact with bone structure leading to dissolution of the latter. Bone distance profile - prosthesis can be used for a diagnosis of this problem.

Starting from the segmented image, we can calculate for each line the width of the empty medullar channel (which is the bone - prostheses distance). Ideally this should be minimum and the prostheses stem should geometrically fit inside the bone. Figure 10 plots the profile of the prosthesis - bone distance on both sides of the stem.

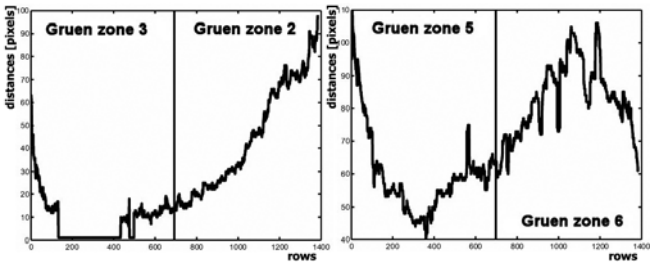

a) b)

Figure 10. Bone-prostheses distance profile on Gruen zones (a) 3 and 2 and respectively (b) 5 and 6 in the case presented in figure 5 (a). The values on the Y axes are the distances in pixels at the corresponding row plotted on the X axis (starting from the end of the stem).

V. Conclusions And Future Steps

The approach described in this paper can be used as automated screening for the follow-up of patients with hip prostheses by standard X-ray investigation, creating a prosthesis evolution history, which could be subsequently used for the prediction of the prosthesis degradation. The mandatory future steps imply the enlargement of the database with more data that addresses a broader range of problems from the THA pathology.

On the other hand, even that all the received feedback was positive, such methods for computer-aided diagnostic must follow a lengthy process before becoming of standard use daily medical practice. Authors are determined to persevere in doing all the necessary steps so to see a practical use of it.

References

[1] "Nationwide inpatient sample," on-line database.

[2] S. Kurtz, K. Ong, E. Lau, F. Mowat, and M. Halpern, "Projections of primary and revision hip and knee arthroplasty in the United States from 2005 to 2030," *Journal of Bone and Joint Surgery*, vol. 89, no. 4, pp. 780–5, 2007.

[3] J. D'Antonio, J. C. McCarthy, W. L. Barger, and et all, "Classification of femoral abnormalities in total hip arthroplasty," *Clinical Orthopaedics and Related Research*, vol. 296, pp. 133–139, 1993.

[4] S. Webb, *The Physics of Medical Imaging*. Institute of Physics Publishing, 1998.

[5] C. Florea, C. Vertan, and L. Florea, "Logarithmic model-based dynamic range enhancement of hip X-ray images," in *Proceedings of Advanced Concepts for Intelligent Vision Systems*. LNCS vol. 4678, 2007, pp. 587–596.

[6] L. Florea, C. Vertan, C. Florea, and A. Oprea, "Dynamic range enhancement of consumer digital camera acquired hip prosthesis xray images," in *Proceedings of European Signal Processing Conference (EUSIPCO)*, Poznan, Poland, September 2007, pp. 1103–1106.

[7] E. Reinhard, G. Ward, S. Pattanaik, and P. Debevec, *High Dynamic Range Imaging: Acquisition, Display and Image-Based Lighting*. San Francisco, California, S.U.A: Morgan Kaufmann Publishers, 2005.

[8] A. PH2.5-1960, "American standard method for determining speed of photographic negative materials (monochrome, continuous tone)," 1960, United States of America Standards Institute.

[9] M. Jourlin and J. C. Pinoli, "A model for logarithmic image processing," *Journal of Microscopy*, vol. 149, no. 1, pp. 21–35, 1998.

[10] R. C. Gonzales and R. E. Woods, *Digital Image Processing,* Addison-Wesley Longman Publishing Co., Inc. Boston, MA, USA, 1992.

[11] D. Coltuc and P. Bolon, "Robust watermarking by histogram specification," in *Proceedings of IEEE International Conference on Image Processing (ICIP)*, no. 2, Kobe, Japan, 1999, pp. 236–239.

[12] A. G. D. Valle and W. G. Paprosky, *Revision total hip arthroplasty*. Orthopaedic Knowledge Online, American Academy of Orthopaedic Surgeons, 2003.

[13] X. Dong, M. Gonzalez-Ballester, and G. Zheng, "Automatic extraction of femur contours from calibrated x-ray images using statistical information," *Journal of Multimedia*, vol. 2, no. 5, pp. 46–54, 2007.

[14] C. Ying, *Model-based approach for extracting femur contours in x-ray images*, Ph.D. dissertation, National University of Singapore, 2005.

[15] F. Hatfield, F. Hall, R. King, E. Berry, P. Siney, and B. Wrobleski, "Image analysis of wear in total hip replacements," in *Proceedings of Medical Image Understanding and Analysis (MIUA)*, Birmingham, Marea Britanie, 2001, pp. 127–131.

[16] S. Kerrigan, S. J. McKenna, I. W. Ricketts, and C. A. Wigderowitz, "Eccentric elliptical contours in total hip replacements," in *Proceedings of Medical Image Understanding and Analysis (MIUA)*, London, Marea Britanie, 2004, pp. 216–219.

[17] S. Kerrigan, S. J. McKenna, I. W. Ricketts, and C. A. Wigderowitz, "Automated assessment of polyethylene wear in cemented acetabular components using anteroposterior radiographs of total hip replacements," in *Proceedings of the Computerized Medical Imaging and Graphics*, vol. 32, no. 3, 2008, pp. 221–238.

[18] N. Otsu, "A threshold selection method from gray level histograms," *IEEE Transactions on System, Man and Cybernetics*, vol. 9, pp. 62–66, 1979.

[19] J. Kitler and J. Illingworth, "Minimum error thresholding," *Journal of Pattern Recognition*, vol. 19, no. 1, pp. 41–47, 1986.

[20] J. Bezdek, *Pattern Recognition with Fuzzy Objective Function Algorithms*. Norwell, MA, SUA: Kluwer Academic Publishers, 1981.

[21] D. Comaniciu and P. Meer, "Mean shift: a robust approach toward feature space analysis," *IEEE Transactions on Pattern Analysis and Machine Intelligence*, vol. 24, no. 5, pp. 603 – 619, 2002.

[22] A. P. Dempster, N. M. Laird, and D. B. Rubin, "Maximum likelihood from incomplete data via the em algorithm," *Journal of the Royal Statistical Society, Series B*, vol. 39, p. 1–38, 1977.

[23] I. E. Sobel, *Camera models and machine perception*, Ph.D. dissertation, Stanford University, Stanford, SUA, 1970.

[24] C. Harris and M. Stephens, "A combined corner and edge detector," in *Proceedings of The Fourth Alvey Vision Conference*, 1988, pp. 147–151.

[25] J. Canny, "A computational approach to edge detection," *IEEE Transaction on Pattern Recognition and Machine Intelligence*, vol. 8, no. 6, pp. 679–698, November 1986.

[26] A. Oprea and C. Vertan, "A quantitative evaluation of the hip prosthesis segmentation quality in X-ray images," in *Proceedings of IEEE International Symposium on Signals, Circuits and Systems (ISSCS)*, vol. 1, Iasi, Romania, July 2007, pp. 197–200.

[27] M. Sezgin and B. Sankur, "Survey over image thresholding techniques and quantitative performance evaluation," *Journal of Electronic Imaging*, vol. 13, no. 1, pp. 146–168, March 2004.

[28] R. A. Redner and H. F. Walker, "Mixture densities, maximum likelihood and the EM algorithm," *SIAM Review*, vol. 26, no. 2, pp. 195–239, April 1984.

[29] M. Nixon and A. Aguado, *Feature Extraction & Image Processing*. Oxford, Great Britain: Newnes, Butterworth-Heinemann Linacre House, 2002.